Electronic Supplementary Material (ESI) for Journal of Materials Chemistry C.
This journal is © The Royal Society of Chemistry 2022

Supporting Information

A Linear Deep-Blue Bipolar Fluorescent Material with the CIEy < 0.065 Serving as Emitter and Host for High-Performance Monochromatic and Hybrid White OLEDs

Ling Peng[a], Yumiao Huo[d], Shuyao He[a], Yuchao Liu[a], Zhongjie Ren[c], Shian Ying[a,b*], Shouke Yan[a,c*]

[a] Key Laboratory of Rubber-Plastics, Ministry of Education, Qingdao University of Science & Technology, Qingdao 266042, P. R. China.

[b] Institute of Polymer Optoelectronic Materials and Devices, State Key Laboratory of Luminescent Materials and Devices, South China University of Technology, Guangzhou 510640, P. R. China.

[c] State Key Laboratory of Chemical Resource Engineering, College of Materials Science and Engineering, Beijing University of Chemical Technology, Beijing 100029, P. R. China.

[d] College of Materials Science and Engineering, Shandong University of Science and Technology, Qingdao 266590, P. R. China.

*Corresponding author: shian0610@126.com; skyan@mail.buct.edu.cn

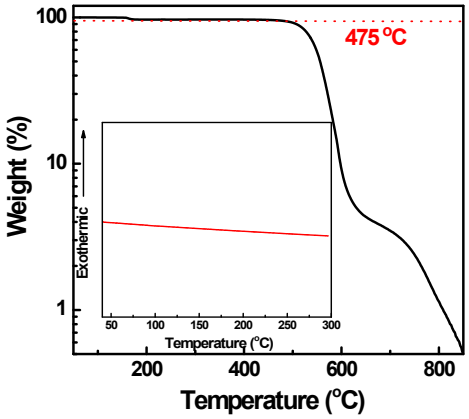

Fig. S1. TGA curve of the compound **P2MPC**. Inset: DSC curve of the compound **P2MPC**.

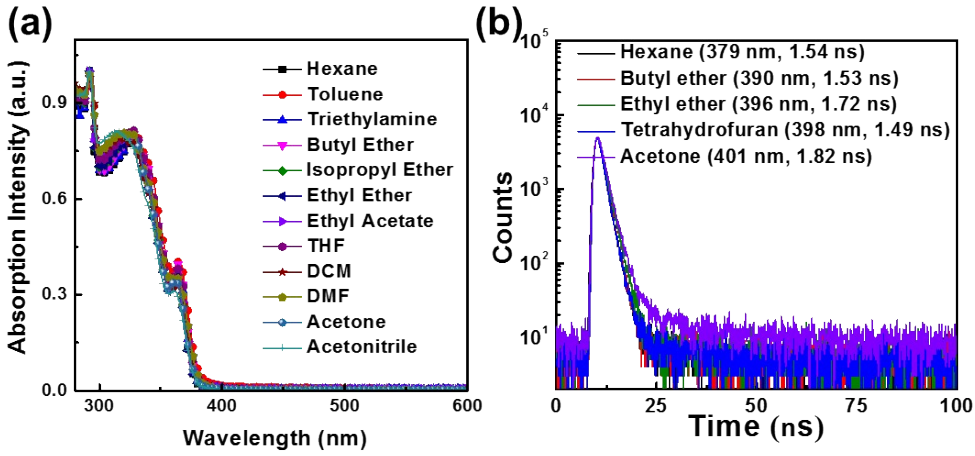

Fig. S2. (a) Absorption spectra of **P2MPC** in the different solvents. (b) Time-resolved PL decay curves in different solvents (10 μM).

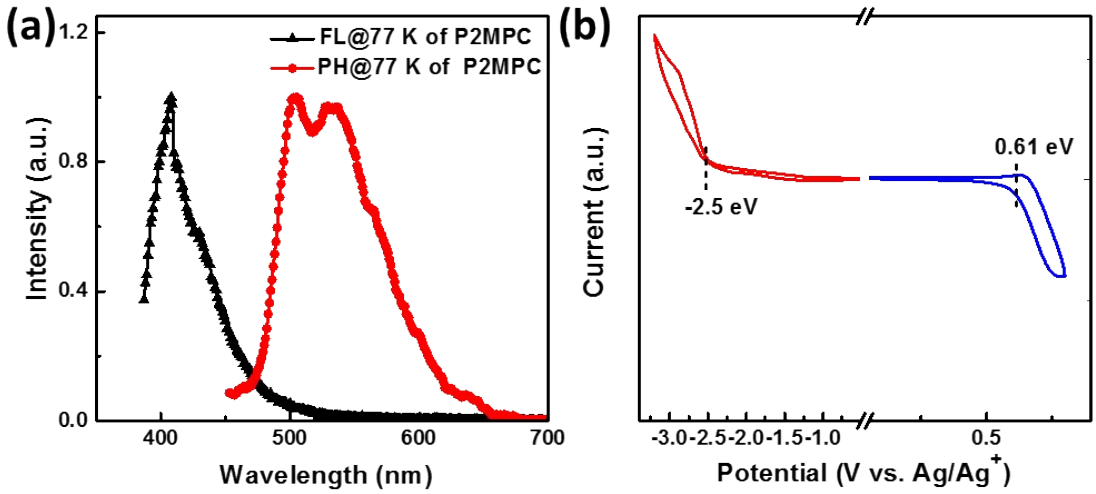

Fig. S3. (a) Fluorescent and phosphorescent spectra of **P2MPC** in dichloromethane solution at 77 K. (b) Cyclic voltammograms curves of **P2MPC**.

Lippert-Mataga Calculation

The Stokes shift ($\nu_A - \nu_{PL}$) versus orientational polarizability ((ε, n)) of solvents can be constructed by the Lippert-Mataga model with the Equation 1 as below.

$$hc(\nu_A - \nu_{PL}) = hc(\nu_A^0 - \nu_{PL}^0) + \frac{2(\mu_e - \mu_g)^2}{a_0^3} f(\varepsilon,n) \quad (1)$$

Here, h is the Plank constant, c is the light speed in vacuum, μ_g and μ_e are the ground-state excited-state dipole moments, (ε, n) is the orientational polarizability of solvents, a_0 is the Onsager cavity radius, $\nu_A^0 - \nu_{PL}^0$ is the Stokes shifts when f is zero, respectively.

Take differential on both sides of the Equation 1, the Equation 2 can be obtained:

$$\mu_e = \mu_g + \{\frac{hca_0^3}{2} \times [\frac{d(\nu_A - \nu_{PL})}{df(\varepsilon,n)}]\}^{1/2} \quad (2)$$

(ε, n) and a_0 can be obtained by the Equation 3 and 4:

$$f(\varepsilon,n) = \frac{\varepsilon - 1}{2\varepsilon + 1} + \frac{n^2 - 1}{2n^2 + 1} \quad (3)$$

$$a_0 = (\frac{3M}{4\pi Nd})^{1/3} \quad (4)$$

Where, ε and n are dielectric constant and refractive index of solvent, N is Avogadro's number, M is molar mass, and d is density of the solvents, respectively. The values of (ε, n) and a_0 can be estimated by the Equation 3 and 4. The μ_g of **P2MPC** (3.97 D) was estimated with the Gaussian 09 package at the level of RB3LYP/6-31G(d, p). The $\frac{d(\nu_A - \nu_{PL})}{df(\varepsilon,n)}$ can be estimated with the solvatochromic experiment data listed in Table S1. With the information above, a linear relationship with the slope of 3905.88 (Correlation = 0.977) was achieved, corresponding to the μ_e of 10.50 D.

Table S1. The detailed absorption, emission peak and of P2MPC in different solvents

Solvents	ε	n	f(ε, n)	λ_A [nm]	λ_{PL} [nm]	ν_A- ν_{PL} [cm^{-1}]
Hexane	1.9	1.375	0.0012	293	379	7744.5
Toluene	2.38	1.494	0.013	293	387	8289.9
Triethylamine	2.42	1.401	0.048	293	396	8877.2
Butyl ether	3.08	1.399	0.096	293	390	8488.7
Isopropyl ether	3.88	1.368	0.145	293	394	8749.0
Ethyl ether	4.34	1.352	0.167	293	396	8877.2
Ethyl acetate	6.02	1.372	0.2	293	398	9004.1
Tetrahydrofuran	7.58	1.407	0.21	293	398	9004.1
Dichloromethane	8.93	1.424	0.217	293	401	9192.0
Dimethylformamide	37	1.427	0.276	293	404	9377.2

Acetone	20.7	1.359	0.284	293	401	9192.0
Acetonitrile	37.5	1.344	0.305	293	405	9438.3

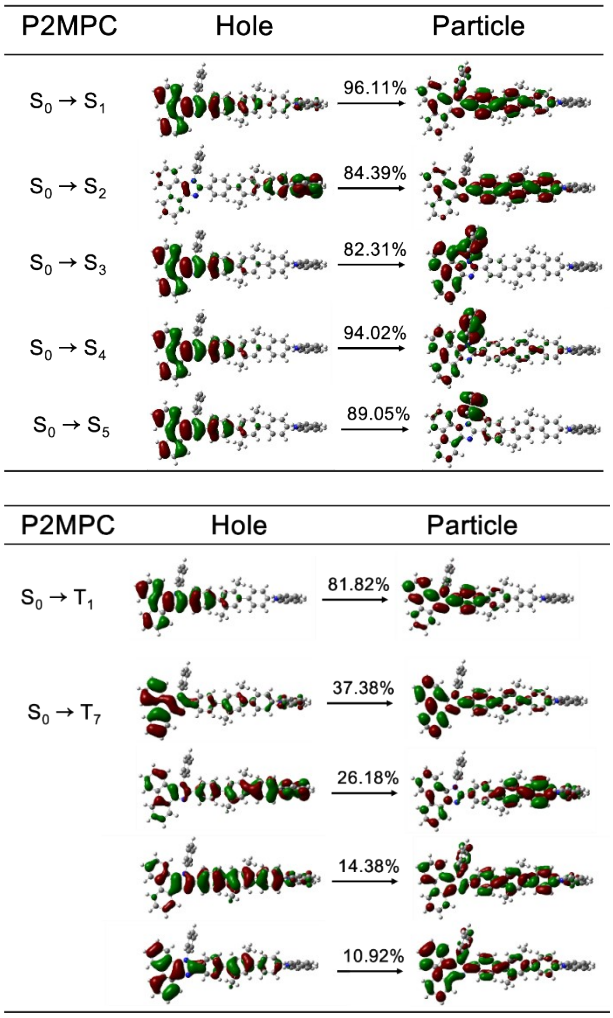

Fig. S4. The NTO transition characters of the singlet and triplet states.

Table S2. Energy levels of singlet and triplet states and oscillator strengths of singlet states in **P2MPC**

Excited States	S energy level [eV]	T energy level [eV]	S Oscillator Strength
1	3.4976	2.6625	1.1834
2	3.7148	3.0132	0.0352
3	3.7214	3.1796	0.0273
4	3.847	3.2029	0.0426
5	3.9397	3.3414	0.0142
6	4.0041	3.3452	0.042
7	4.0396	3.4843	0.0057
8	4.1192	3.5984	0.0909
9	4.1562	3.6789	0
10	4.2143	3.7613	0.0361

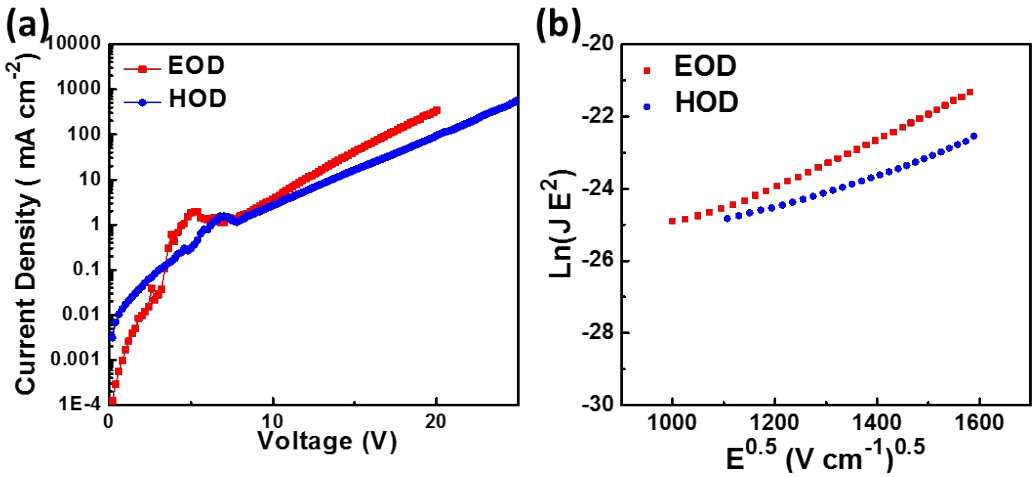

Fig. S5. Current density–voltage characteristics (a), and In (J E^{-2})–$E^{0.5}$ characteristics (b) of hole- and electron-only devices.

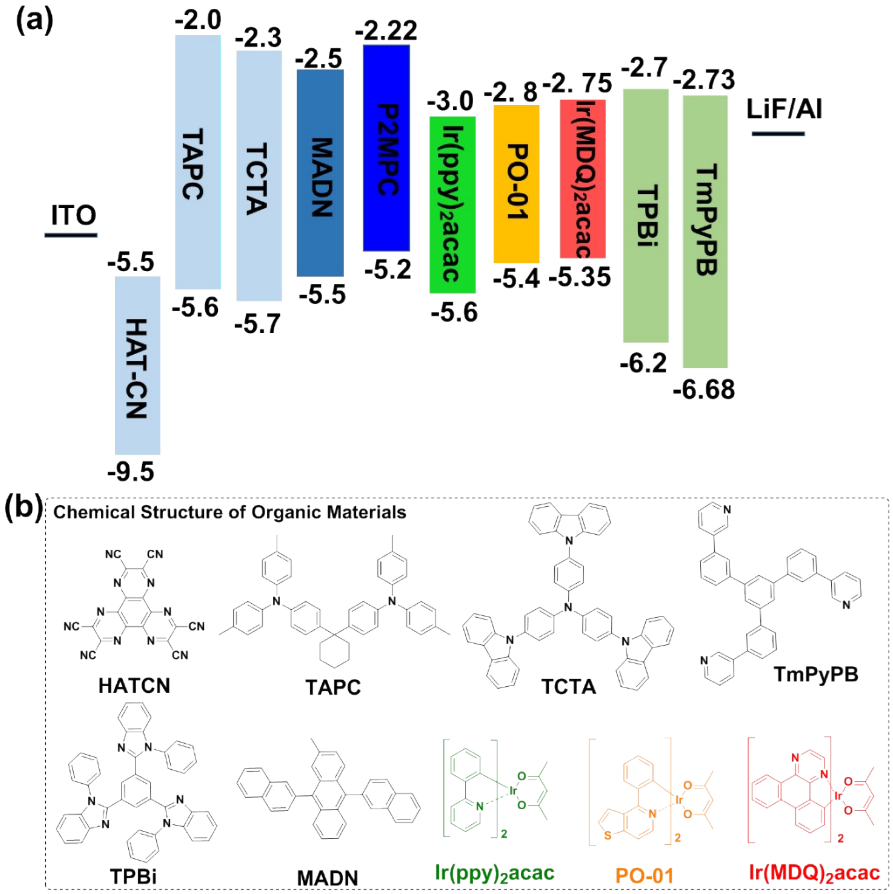

Fig. S6. The energy level diagrams and molecular structures of organic materials used in the devices.

Table S3. Summary of EL performance of reported high-performance non-doped deep-blue OLEDs with CIEy $\leqslant$ 0.07.

Ref.	L_{max} [a] [cd m^{-2}]	EQE_{max} [a] [%]	EQE_{100} [a] [%]	EQE_{1000} [a] [%]	CIE(x,y)
This work	**6331**	**7.15**	**6.80**	**5.65**	**(0.157, 0.064)**
Ref.1	5146	6.4	6.13	5.58	(0.151, 0.066)
	5382	5.87	5.76	5.52	(0.148, 0.070)
Ref.2	-	5.08	5.00	4.44	(0.16, 0.06)
	-	4.47	4.45	4.13	(0.16, 0.07)
Ref.3	2233	5.3		4.2	(0.16, 0.06)
	2445	7.1		5.3	(0.16, 0.06)
Ref.4	3113	6.57	4.04	-	(0.17, 0.07)
Ref.5	1890	1.97	-	-	(0.16, 0.06)
Ref.6	-	8.9	3.9 [b]	-	(0.150, 0.060)
Ref.7	4543	3.02	-	-	(0.167, 0.056)
	3602	1.51	-	-	(0.165, 0.053)
	3342	1.94	-	-	(0.165, 0.050)
Ref.8	-	3.38	-	-	(0.154, 0.063)
Ref.9	8951	5.29	-	-	(0.155, 0.058)
Ref.10	2690	4.18			(0.154,0.042)
	7490	5.74	5.50	4.80	(0.152,0.054)
Ref.11	9163	4.21		3.83	(0.152, 0.057)
	9165	4.60		4.04	(0.154, 0.058)
Ref.12	8024	3.19	-	-	(0.156, 0.054)
Ref.13	18 105	6.33	-	6.32	(0.151, 0.066)
Ref.14	-	4	-	-	(0.157,0.053)
	-	2.6		-	(0.158,0.045)
Ref.15	-	4.34	3.9	-	(0.160, 0.035)
	-	4.78	4.59	-	(0.159, 0.060)
	-	2.76	2.24	-	(0.167, 0.070)
Ref.16	15560	4.12	-	3.3	(0.160, 0.038)
	4916	6.49	-	4.36	(0.156, 0.046)
	3822	6.73	-	4.01	(0.156, 0.055)

[a] L_{max}, EQE_{max}, $EQE_{100,}$ and EQE_{1000} represent the maximum luminance and external quantum efficiencies at the maximum and 100 and 1000 cd m^{-2}; [b] external quantum efficiency at 500 cd m^{-2}.

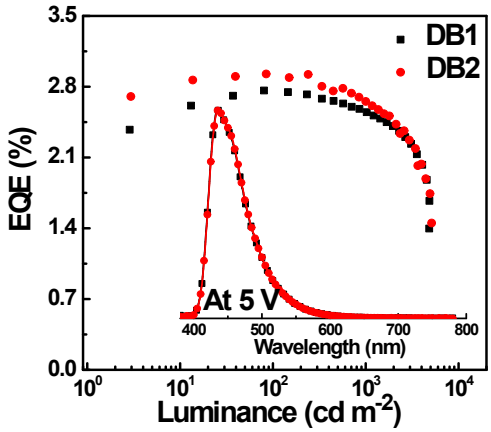

Fig. S7. EQE versus luminance characteristics of the devices **DB1** and **DB2** with the structure of ITO/ HATCN (20 nm)/ TAPC (50 nm)/ TCTA (5 nm)/ MADN: **P2MPC** (XX, 20 nm)/ TPBi (10 nm)/ TmPyPB (35 nm)/ LiF (1 nm)/Al (100 nm), where the doping concentrations of 2 and 10 wt% for **DB1** and **DB2**. Inset: the EL spectra at the applied voltage of 5 V.

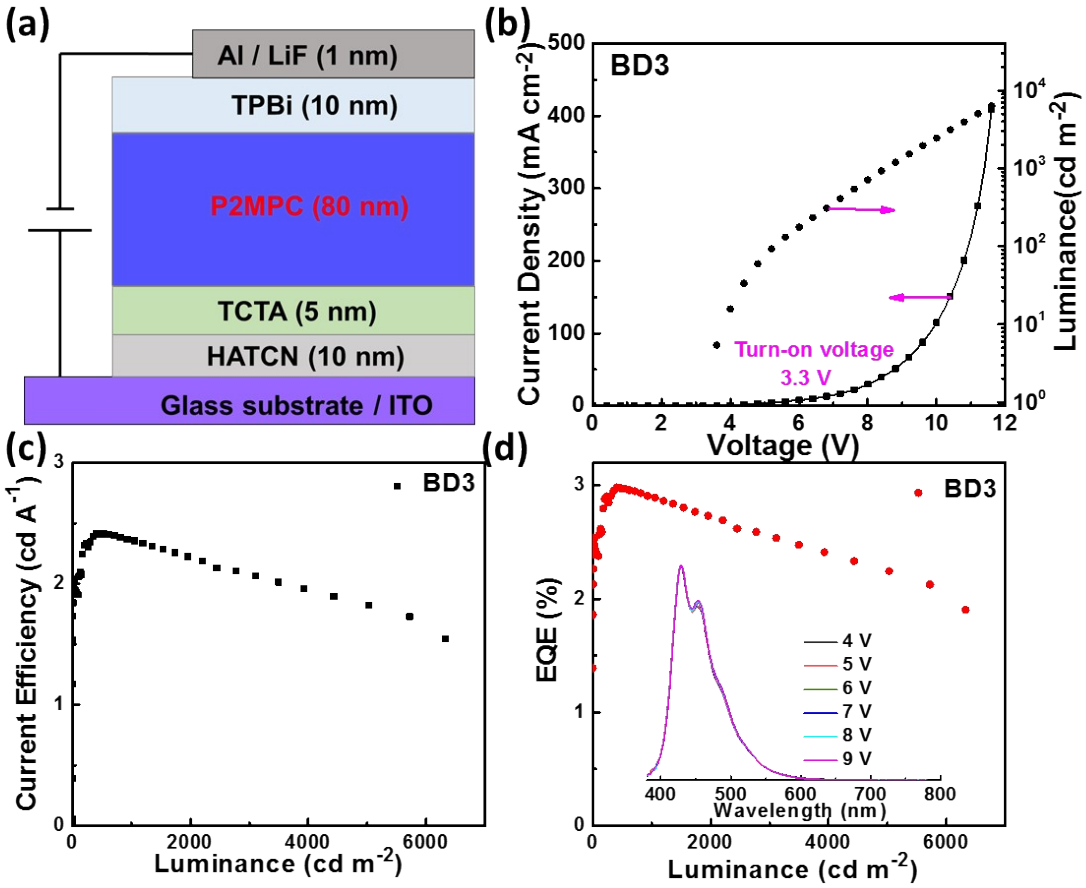

Fig. S8. Device configuration and EL performance of the non-doped OLED **BD3**. (a) Device configuration. (b) Current density-voltage-luminance characteristics. (c) Current efficiency as a function of luminance. (d) EQE versus luminance characteristic. Inset: the EL spectra with different applied voltages.

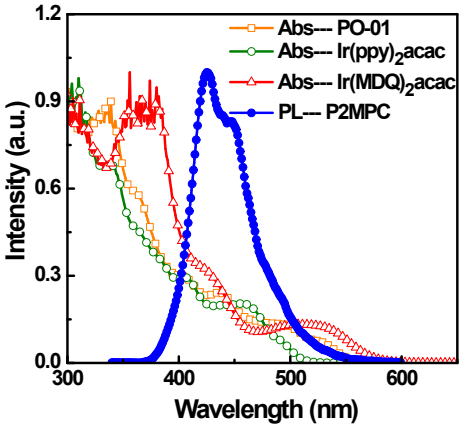

Fig. S9. Absorption spectra of $Ir(ppy)_2acac$, PO-01 and $Ir(MDQ)_2acac$ in dichloromethane solution and PL spectrum of **P2MPC** in film.

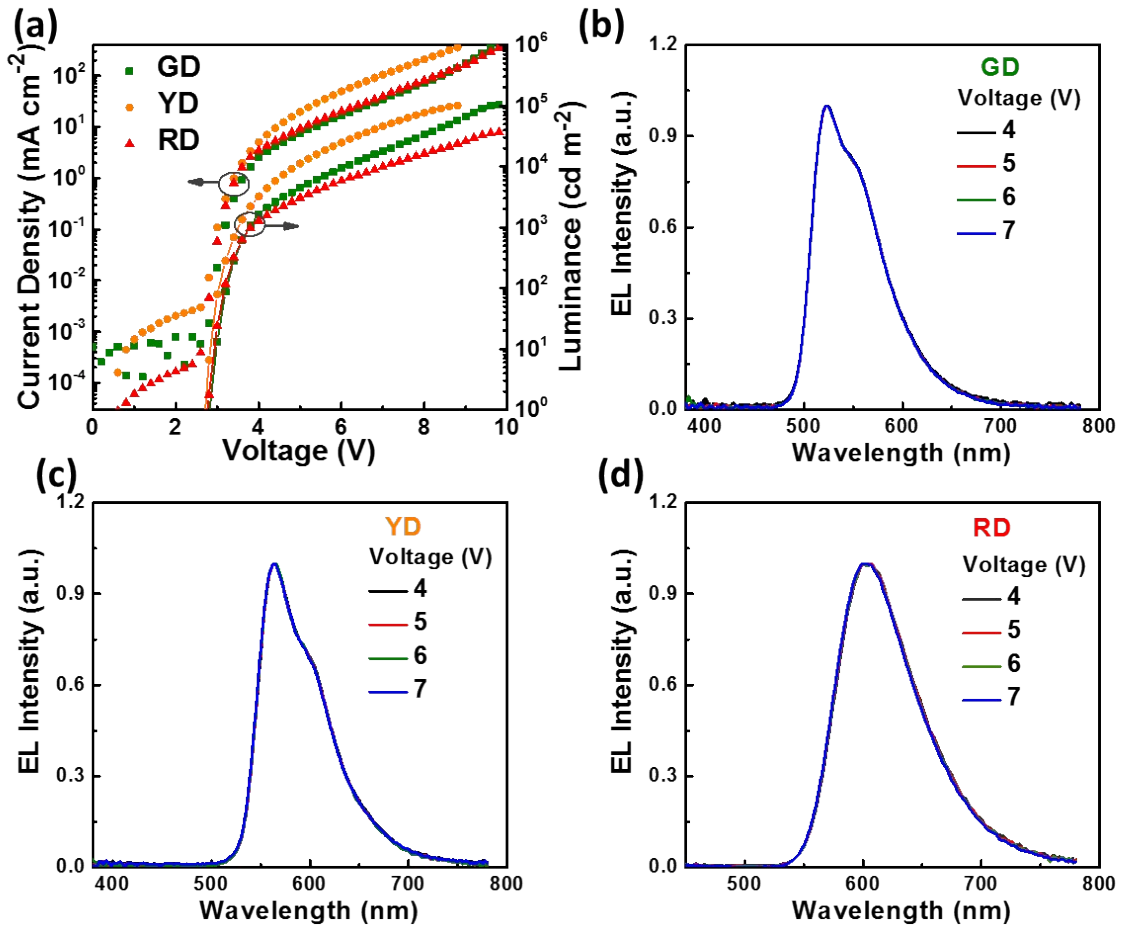

Fig. S10. (a) Current density-voltage-luminance characteristics of the devices **GD**, **YD**, and **RD**. (b) The EL spectra of the device **GD** at the different applied voltages. (c) The EL spectra of the device **YD** at the different applied voltages. (d) The EL spectra of the device **RD** at the different applied voltages. The device structure of **GD** is ITO/ HATCN (20 nm)/ TAPC (50 nm)/ TCTA (5 nm)/ **P2MPC**: $Ir(ppy)_2acac$ (10 wt%, 20 nm)/ TPBi (45 nm)/ LiF (1 nm)/Al (100 nm). The device structure of **YD** is ITO/ PEDOT:PSS (30 nm)/ TAPC (40 nm)/ TCTA (5 nm)/ **P2MPC**: PO-01 (5 wt%, 20 nm)/ TPBi (10 nm)/ TmPyPB (30 nm)/ LiF (1 nm)/Al (100 nm). The device structure of **RD** is ITO/ HATCN (20 nm)/ TAPC (50 nm)/ TCTA (5 nm)/ **P2MPC**: $Ir(MDQ)_2acac$ (5 wt%, 20 nm)/ TPBi (45 nm)/ LiF (1 nm)/Al (100 nm).

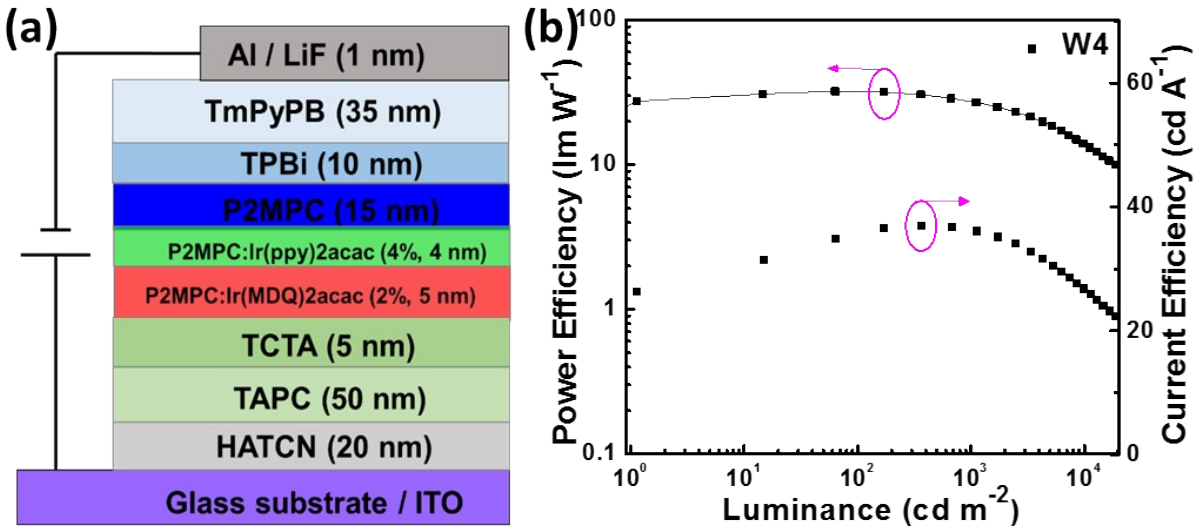

Fig. S11. (a) Device configuration of the device **W4**. (b) Power efficiency and current efficiency as a function of luminance based on the device **W4**.

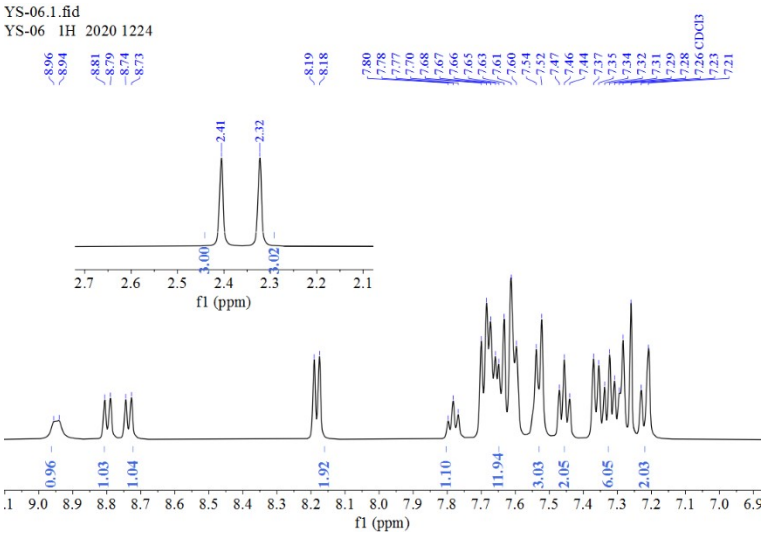

Fig. S12. ^{1}H NMR spectrum of the target compound **P2MPC**.

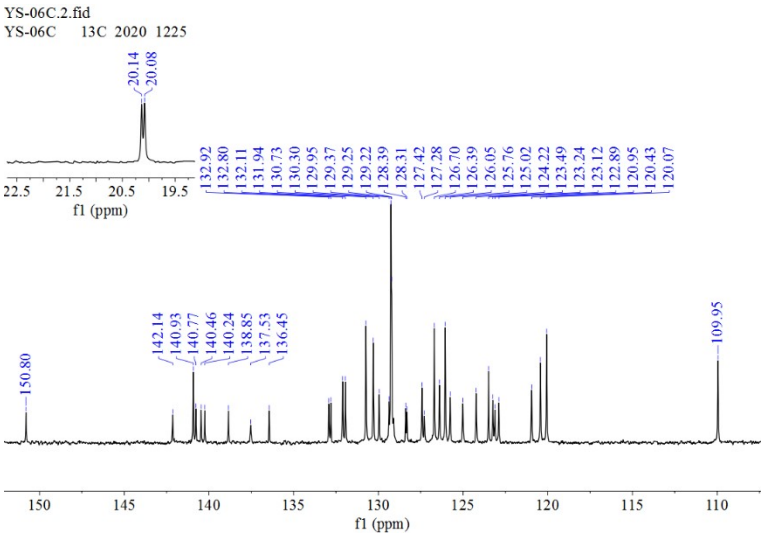

Fig. S13. ^{13}C NMR spectrum of the target compound **P2MPC**.

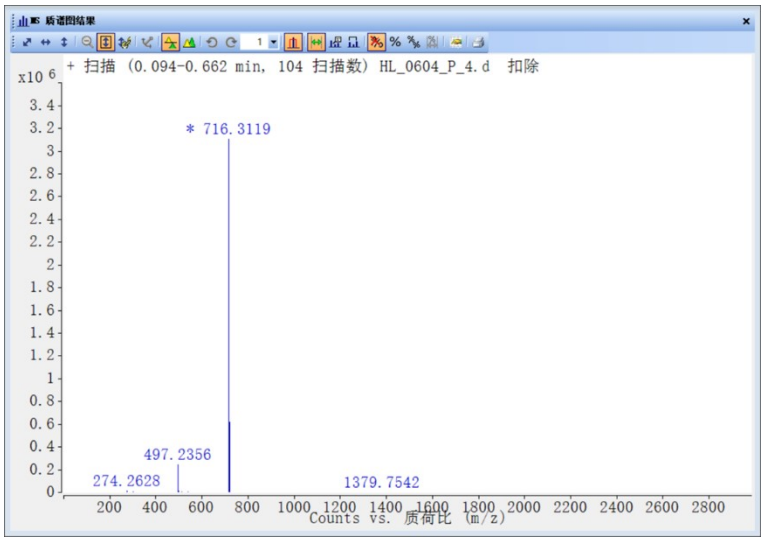

Fig. S14. HRMS spectrum of the target compound **P2MPC**.

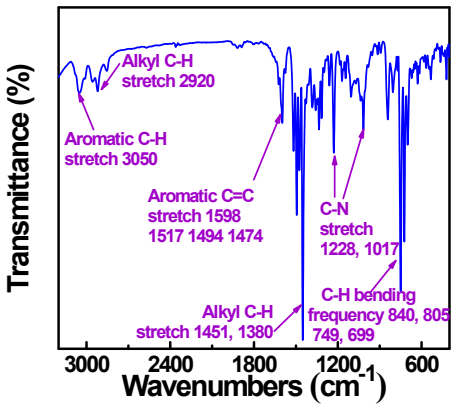

Fig. S15. Infrared (IR) spectrum of the target compound **P2MPC**.

Detailed Study of RISC Process for P2MPC

The possibility of thermally activated delayed fluorescence (TADF) process can be ruled out due to the nanosecond-scale single-exponential decay lifetime and large ΔE_{ST} (**Fig. 1b, S2b**), while the good linear correlation between luminance and current density implies that the triplet-triplet annihilation (TTA) process is not the main emission mechanism for the device **BD** (**Fig. S16b**). According to the natural transition orbitals (NTOs) of P2MPC, the excited states of S_1, and T_7 show HLCT transition character, which ensure the existence of high-lying reverse intersystem crossing (hRISC) process. Meanwhile, from the analysis of Lippert-Mataga solvatochromic model and nanosecond-scale single-exponential decay lifetimes in different solvents, the HLCT character of P2MPC can be confirmed. Furthermore, as shown in **Fig. S16a**, large ΔE_{ST} of 0.8351 eV between S_1 and T_1, and small energy differences of 0.0133 eV between S_1 and T_7 can effectively enhance the hRISC rate, making more singlet excitons be generated via hRISC channel.

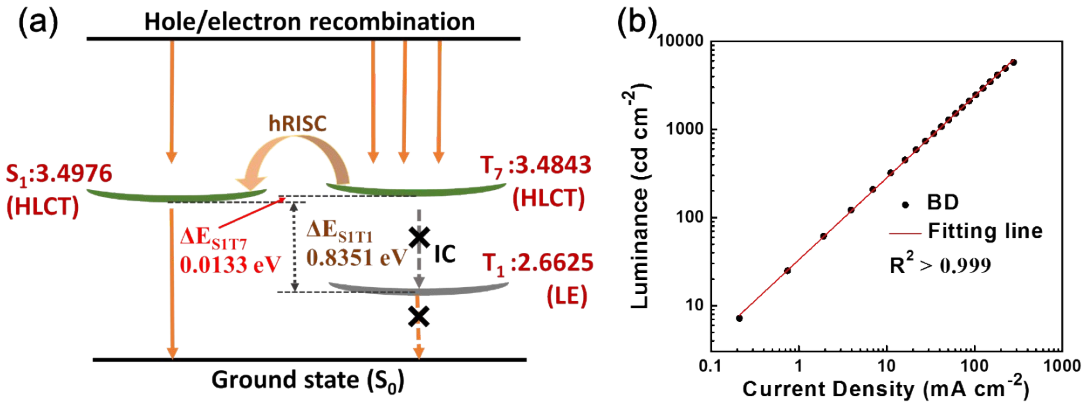

Fig. S16. (a) Probable emission mechanism of HLCT material **P2MPC**. S: singlet state; T: triplet state; LE: local excited state; ΔE_{ST}: singlet–triplet energy splitting; IC: internal conversion; hRISC: high-lying reverse intersystem crossing. (b) Luminance versus current density curve of the device BD. The fitting line of y = 0.92938x + 1.52109.

References

[1] Ye, S.; Wang, Y.; Guo, R.; Zhang, Q.; Lv, X.; Duan, Y.; Leng, P.; Sun, S.; Wang, L. Asymmetric anthracene derivatives as multifunctional electronic materials for constructing simplified and efficient non-doped homogeneous deep blue fluorescent OLEDs. *Chem. Eng. J.* **2020**, *393*, 124694.

[2] Zhu, Z.-L.; Ni, S.-F.; Chen, W.-C.; Chen, M.; Zhu, J.-J.; Yuan, Y.; Tong, Q.-X.; Wong, F.-L.; Lee, C.-S. Tuning electrical properties of phenanthroimidazole derivatives to construct multifunctional deep-blue electroluminescent materials. *J. Mater. Chem. C* **2018**, *6*, 3584-3592.

[3] Zheng, Y.; Zhu, X.; Ni, Z.; Wang, X.; Zhong, Z.; Feng, X. J.; Zhao, Z.; Lu, H. Bipolar Molecules with Hybridized Local and Charge-Transfer State for Highly Efficient Deep-Blue Organic Light-Emitting Diodes with EQE of 7.4% and CIEy∼ 0.05. *Adv. Opt. Mater.* **2021**, *9*, 2100965.

[4] Xue, S.; Qiu, X.; Ying, S.; Lu, Y.; Pan, Y.; Sun, Q.; Gu, C.; Yang, W. Highly Efficient Nondoped Near-Ultraviolet Electroluminescence with an External Quantum Efficiency Greater Than 6.5% Based on a Carbazole–Triazole Hybrid Molecule with High and Balanced Charge Mobility. *Adv. Opt. Mater.* **2017**, *5*, 1700747.

[5] Jhulki, S.; Mishra, A. K.; Ghosh, A.; Chow, T. J.; Moorthy, J. N. Deep blue-emissive bifunctional (hole-transporting + emissive) materials with CIEy ∼ 0.06 based on a 'U'-shaped phenanthrene scaffold for application in organic light-emitting diodes. *J. Mater. Chem. C* **2016**, *4*, 9310-9315.

[6] Huh, J.-S.; Ha, Y. H.; Kwon, S.-K.; Kim, Y.-H.; Kim, J.-J. Design Strategy of Anthracene-Based Fluorophores toward High-Efficiency Deep Blue Organic Light-Emitting Diodes Utilizing Triplet–Triplet Fusion. *ACS Appl. Mater. Interfaces* **2020**, *12*, 15422-15429.

[7] Gao, Z.; Wang, Z.; Shan, T.; Liu, Y.; Shen, F.; Pan, Y.; Zhang, H.; He, X.; Lu, P.; Yang, B.; Ma, Y. High-efficiency deep blue fluorescent emitters based on phenanthro[9,10-d]imidazole substituted carbazole and their applications in organic light emitting diodes. *Org. Electron.* **2014**, *15*, 2667-2676.

[8] Chen, W.-C.; Yuan, Y.; Ni, S.-F.; Tong, Q.-X.; Wong, F.-L.; Lee, C.-S. Achieving efficient violet-blue electroluminescence with CIEy <0.06 and EQE >6% from naphthyl-linked phenanthroimidazole–carbazole hybrid fluorophores. *Chem. Sci.* **2017**, *8*, 3599-3608.

[9] Wang, Z.-Y.; Zhao, J.-W.; Liu, B.; Cao, C.; Li, P.; Tong, Q.-X.; Tao, S.-L. Universal materials for high performance violet-blue OLEDs (CIEy < 0.06) and PhOLEDs. *Dyes Pigm.* **2019**, *163*, 213-220.

[10] Qiu, X.; Ying, S.; Wang, C.; Hanif, M.; Xu, Y.; Li, Y.; Zhao, R.; Hu, D.; Ma, D.; Ma, Y. Novel 9,9-dimethylfluorene-bridged D–π–A-type fluorophores with a hybridized local and charge-transfer excited state for

deep-blue electroluminescence with CIEy ~ 0.05. *J. Mater. Chem. C* **2019**, *7*, 592-600.

[11] Zhao, J.; Liu, B.; Wang, Z.; Tong, Q.; Du, X.; Zheng, C.; Lin, H.; Tao, S.; Zhang, X. EQE Climbing Over 6% at High Brightness of 14350 cd/m2 in Deep-Blue OLEDs Based on Hybridized Local and Charge-Transfer Fluorescence. *ACS Appl. Mater. Interfaces* **2018**, *10*, 9629-9637.

[12] Zhou, H.; Yin, M.; Zhao, Z.; Miao, Y.; Jin, X.; Huang, J.; Gao, Z.; Wang, H.; Su, J.; Tian, H. Novel carbazole-based multifunctional materials with a hybridized local and charge-transfer excited state acting as deep-blue emitters and phosphorescent hosts for highly efficient organic light-emitting diodes. *J. Mater. Chem. C* **2021**, *9*, 5899-5907.

[13] Liu, B.; Yu, Z.-W.; He, D.; Zhu, Z.-L.; Zheng, J.; Yu, Y.-D.; Xie, W.-F.; Tong, Q.-X.; Lee, C.-S. Ambipolar D–A type bifunctional materials with hybridized local and charge-transfer excited state for high performance electroluminescence with EQE of 7.20% and CIEy ~ 0.06. *J. Mater. Chem. C* **2017**, *5*, 5402-5410.

[14] Xiao, S.; Zhang, S.-T.; Gao, Y.; Yang, X.; Liu, H.; Li, W.; Yang, B. Efficient and stable deep-blue narrow-spectrum electroluminescence based on hybridized local and charge-transfer (HLCT) state. *Dyes Pigm.* **2021**, *193*, 109482.

[15] Han, P.; Lin, C.; Ma, D.; Qin, A.; Tang, B. Z. Violet-Blue Emitters Featuring Aggregation-Enhanced Emission Characteristics for Nondoped OLEDs with CIEy Smaller than 0.046. *ACS Appl. Mater. Interfaces* **2020**, *12*, 46366-46372.

[16] Li, Z.; Xie, N.; Xu, Y.; Li, C.; Mu, X.; Wang, Y. Fluorine-Substituted Phenanthro[9,10-d]imidazole Derivatives with Optimized Charge-Transfer Characteristics for Efficient Deep-Blue Emitters. *Org. Mater.* **2020**, *02*, 011-019.